Optimized reaction mechanism rate rules for ignition of normal alkanes

Liming Cai[a,*], Heinz Pitsch[a], Samah Y. Mohamed[b], Venkat Raman[c], John Bugler[d], Henry Curran[d], S. Mani Sarathy[b]

[a] *Institute for Combustion Technology, RWTH Aachen University, 52062 Aachen, Germany*
[b] *Clean Combustion Research Center, King Abdullah University of Science and Technology, Thuwal 23955-6900, Saudi Arabia*
[c] *Department of Aerospace Engineering, University of Michigan, Ann Arbor 48109, USA*
[d] *Combustion Chemistry Centre, National University of Ireland, Galway, Ireland*

Abstract

The increasing demand for cleaner combustion and reduced greenhouse gas emissions motivates research on the combustion of hydrocarbon fuels and their surrogates. Accurate detailed chemical kinetic models are an important prerequisite for high fidelity reacting flow simulations capable of improving combustor design and operation. The development of such models for many new fuel components and/or surrogate molecules is greatly facilitated by the application of reaction classes and rate rules. Accurate and versatile rate rules are desirable to improve the predictive accuracy of kinetic models. A major contribution in the literature is the recent work by Bugler et al. (Bugler et al., J. Phys. Chem. A 119 (2015) 7510-7527), which has significantly improved rate rules and thermochemical parameters used in kinetic modeling of alkanes. In the present study, it is demonstrated that rate rules can be used

*Corresponding author:
Email address: lcai@itv.rwth-aachen.de (Liming Cai)

and consistently optimized for a set of normal alkanes including n-heptane, n-octane, n-nonane, n-decane, and n-undecane, thereby improving the predictive accuracy for all the considered fuels. A Bayesian framework is applied in the calibration of the rate rules. The optimized rate rules are subsequently applied to generate a mechanism for n-dodecane, which was not part of the training set for the optimized rate rules. The developed mechanism shows accurate predictions compared with published well-validated mechanisms for a wide range of conditions.

Keywords:

n-Alkanes, Rate Rules, Mechanism Development, Optimization and Uncertainty Quantification

---

1. Introduction

Computational fluid dynamic (CFD) calculations of reactive flows have become an important part in the design of combustion devices. A critical factor in performing successful CFD simulations is an adequate representation of fuel chemistry, especially when more complex phenomena are studied, such as auto-ignition, flame stabilization, or pollutant formation. While chemical mechanisms of several species, e. g. methane, ethanol, and n-heptane, have been extensively studied in the last few years, the accuracy of the mechanisms for most species requires improvement. Furthermore, there is a growing demand for accurate mechanisms of fuel species that have never been studied. Recently, various new surrogate components, such as n-decane [1], n-dodecane [2, 3], and 2,5-dimethylhexane [4] have been proposed to improve the performance of surrogate mixtures for petroleum fuels. Moreover, lim-

ited fossil fuel reserves and a need for renewable energy raise the interest in alternative biofuels. For both kinds of species, mechanisms are generally missing in the literature, which impedes CFD simulations for technical devices burning these fuels. Therefore, the development of accurate chemical reaction schemes becomes even more important, especially for species which have not yet been well studied.

Most chemical mechanisms are still compiled manually [5–11], while several automatic mechanism generation tools have been presented in the literature [12, 13]. The approaches employed in both manual and automatic developments generally rely on the concept of reaction classes and rate rules. In this concept, the fuel specific oxidation steps are described by classes of reactions with the assigned rate constants. Reaction rate constants can be determined from quantum chemistry calculations [14–18] or experimental measurements [19–21]. However, while this is practical and desirable for several very important reactions, it is experimentally and computationally difficult to determine the rate constants of all involved reactions due to their large number. Therefore, for the chemical reactions without rate data from theory or experiment, rate rules are used to specify their rate constant expressions.

Several studies have focused on the development of accurate rate rules. The addition of molecular oxygen to the fuel radicals, which initializes the low temperature oxidation pathway, was studied by Miyoshi [22]. Villano et al. [23, 24] investigated the isomerization rates of alkyl peroxy (RO_2) and peroxy alkylhydroperoxide (O_2QOOH) radicals for C_2–C_5 alkanes and suggested to use the obtained data also as rate rules for larger hydrocarbon fuels. Due

to their importance, the H-atom migration reactions of RO_2 and O_2QOOH radicals were investigated by Miyoshi [25] and Sharma et al. [26] as well. Also for the decomposition channels of RO_2 and hydroperoxy alkyl (QOOH) radicals, rate rules were determined by Villano et al. [24] and Miyoshi [25]. Recently, Bugler et al. [27] evaluated the results [22–26, 28–34] obtained from various levels of quantum theory and then suggested rate rules for the low-temperature oxidation of alkanes. More importantly, the recommended rate rules were provided with their estimated uncertainties [27].

The knowledge of reaction rate coefficient uncertainties is important, as it can certainly have an impact on prediction accuracy. Uncertainties may come from different sources, for example due to approximations in quantum chemistry calculations or inherent uncertainties in the experimental determination of rate coefficients. While the application of higher levels of quantum theory and the upgrade of measurement facilities may improve the accuracy of rate coefficients, uncertainties still exist. Also the process of parameter optimization depends critically on quantified uncertainties, since modifications to rate coefficients should be made in such a process only within the uncertainty limits.

Rate coefficients are often tuned during model development. For this, the important reactions are typically first identified by sensitivity analyses at conditions of interest. Then, the rate parameters for these reactions are modified manually and iteratively within their uncertainty limits to achieve good agreement between model and experiment. In recent years, automatic optimization and uncertainty quantification (UQ) techniques have been successfully established for improving predictive accuracy of chemical mecha-

nisms [35–39]. In cases of rate parameter optimizations found in the literature, rate coefficients of elementary reactions are systematically calibrated. However, the rate parameters of most reactions in chemical mechanisms of larger fuels are adapted using rate rules. A large number of reactions could have identical rate parameters, as they are kinetically similar and therefore follow the same rate rule. Obviously, it is not chemically reasonable to tune rate parameters of individual elementary reactions, as this will violate consistency of kinetically similar reactions. Recently, Cai and Pitsch [40] proposed an automatic mechanism optimization method based on rate rules. This kind of optimization based on group analysis becomes especially important where the concept of analogy in terms of reaction classes and rate rules is used, e. g. also for the development of polycyclic aromatic hydrocarbon formation and growth chemistry [41].

Cai and Pitsch [40] demonstrated the mechanism optimization method based on rate rules by optimizing the model performance of an n-pentane mechanism. The method was later applied to calibrate a chemical mechanism for Primary Reference Fuel (PRF) combustion, in which common rate rules were incorporated for n-heptane and iso-octane [42]. It was shown that, once the common rate rules were automatically calibrated, both reaction schemes were improved. This indicated the possibility to develop optimized universal rate rules, with which accurate chemical mechanisms can be derived for a set of fuels rather than for only one particular fuel.

An additional aspect of optimization and uncertainty quantification is to extract useful information from available data. Typically, experimental data sets are required for model validation. However, despite the increasing inter-

est in long chain fuel species, limited measurements have been performed for them in the literature. The lack of information makes it difficult to derive accurate mechanisms for these fuels of interest. An uncertainty quantification framework gains information from the available measurements for shorter fuels to update the knowledge about rate rules. Once these constrained rate rules are used to construct chemical models of longer chain fuels, the derived models inherit the information from the shorter ones. This creates confidence in the prediction accuracy of mechanisms that cannot be extensively validated due to the lack of experimental measurements.

In this study, it is demonstrated that rate rules calibrated automatically for a number of smaller fuels can be applied in the model development of similar but larger hydrocarbons, yielding predictions that are improved compared to published mechanisms for the same fuel. For this purpose, the rate rules for normal alkanes are studied here. A training of the rate rules is first performed, where the rate rules for n-alkanes are optimized against a large experimental database for n-heptane, n-octane, n-nonane, n-decane, and n-undecane using a Bayesian framework. As a test case, the optimized rate rules are subsequently employed to derive a chemical mechanism for n-dodecane. The derived n-dodecane mechanism is then compared with experimental measurements, a published well-validated mechanism [43], and a mechanism developed with rate rules previously provided in the literature [8, 27]. The validity of the optimized rate rules is thus examined, and the predictive quality of the application of the optimized rate rules in the development of chemical mechanisms for different fuels is demonstrated.

The presentation of this paper is organized as follows. First, the op-

timization methodology based on rate rules is briefly introduced. Next, a mechanism for C_7-C_{11} normal alkanes is developed with the up-to-date kinetic knowledge. Following this, the automatic calibration of the applied rate rules is performed. The article closes with the validation of the *n*-dodecane mechanism developed based on the optimized rate rules.

2. Methodology

Recently, Cai and Pitsch [40] extended the methods by Sheen and Wang [37] and Frenklach [35] for automatic calibration of chemical kinetic models by performing optimization of reaction rate rules. The methodology leads to a chemically more consistent model calibration and improves the model prediction accuracy significantly. As it categorizes chemically similar reactions into one calibration objective, the number of uncertain parameters decreases. This strongly reduces the computational effort of the optimization process and therefore enables optimization of low temperature auto-ignition, where many chemical reactions appear as important. The method was first applied to calibrate an *n*-pentane mechanism [40] and afterwards employed to improve a chemical mechanism for *n*-heptane and iso-octane mixtures, in which common rate rules are incorporated for both fuels [42]. Once the common rate rules are calibrated, both reaction schemes for *n*-heptane and iso-octane are optimized. As the number of rate rules does not increase with the number of fuels in the mechanism, the computational advantage is further advanced. The methodology is described briefly in this section.

2.1. Reaction classes and rate rules

In the present model development process, the fuel specific chemistry of large hydrocarbon fuels is developed based on the approach of using reaction classes and rate rules. Many reaction mechanisms have been built recently in this manner for fuels of interest [5–11]. For these developments, 30 reaction classes, listed in the Supplementary material, were used to derive the chemical mechanisms [8].

Rate rules are employed in this approach to specify the rate constant expressions for the individual elementary reactions provided by the reaction classes. The rate rules for the individual classes were determined based on available chemical kinetic knowledge [5, 8]. If the reactions in a class are carbon site specific or their strain energy barriers are sensitive to the size of transition state rings, several rate rules can be found within this class (e. g. Class 15: RO_2 = QOOH). For reaction classes with limited information of similar reaction types (e. g. Class 16: RO_2 = alkene + HO_2), only one rate rule is employed. In the optimization method proposed by Cai and Pitsch [40], each rate rule is supposed to be a potential active parameter of the model calibration. Once a rate rule is calibrated, the rate constants of all reactions using this rule are consistently modified.

2.2. Optimization algorithm

In previous studies [40, 42], the method of uncertainty minimization using polynomial chaos expansion (MUM-PCE) proposed by Sheen and Wang [37] has been successfully used to calibrate the rate rules and to estimate their uncertainties. MUM-PCE estimates posterior probability density functions (PDFs) of parameters by assuming that these PDFs are either normally or

uniformly distributed [37]. The means of the optimized parameters are determined based on the optimization approach developed originally by Frenklach [35], and the covariance matrix is then estimated analytically. MUM-PCE can be seen as a simplified form of the Bayesian approach for uncertainty quantification, which is exempted from the assumption of a particular form for posterior PDFs. In this study, instead of MUM-PCE, the Bayesian approach is applied to optimize the rate rules, to quantify their uncertainties, and to minimize the model uncertainties.

2.2.1. Bayesian approach

The Bayes' theorem provides a probabilistic approach to gain information about model parameters from given experimental data. In many cases, the exact values of model quantities are unknown, but some information about these parameters has been gained already. Within the Bayesian interpretation, model parameters are treated as random variables and therefore, the state of knowledge about the parameter values can be represented by the PDF of the random variables. The knowledge of these parameters in terms of joint PDFs can be updated with new data according to Bayes' theorem [44, 45].

In probability theory and statistics, the Bayes' theorem [44, 45] states for the given quantities a and b that

$$p(a|b) = \frac{p(a)p(b|a)}{p(b)} \quad , \tag{1}$$

where $p(a)$ and $p(b)$ are the probability distributions of a and b, respectively. $p(a|b)$ is the probability distribution of a conditioned on a specific value of b. Let η^{obs} denote a set of experimental measurements and x be a set of model parameters, then with the notations introduced below, the Bayes' theorem

implies that

$$p_{\text{post}}(x|\eta^{\text{obs}}) = \frac{p_{\text{prior}}(x)\pi(x;\eta^{\text{obs}})}{\int p_{\text{prior}}(x)\pi(x;\eta^{\text{obs}})\mathrm{d}x} \quad . \tag{2}$$

Here, p_{prior} is the prior PDF, which quantifies available information about the parameters x. While this information may incorporate knowledge from previously performed experiments, it is independent of the current experimental data set η^{obs}. In the literature, uniform and Gaussian-shaped PDF forms are most commonly used as priors [46]. A uniform prior assigns a constant probability density to the parameter values within given boundaries, while a Gaussian prior assigns higher density near the mean. p_{post} denotes the posterior PDF, which quantifies the parameter knowledge after incorporating the information from the experimental data η^{obs}. The likelihood function $\pi(x;\eta^{\text{obs}})$ quantifies the agreement between the model and the data for specific values of the parameters:

$$\pi(x;\eta^{\text{obs}}) = p_{\text{like}}(\eta|x)|_{\eta=\eta^{\text{obs}}} \, . \tag{3}$$

In Eq. (3), η is the model prediction. Due to inadequacies in the model (model error) and due to inadequacies in the measurement process (experimental error), the model predictions differ from the observed values. The PDF p_{like} represents the state of knowledge regarding these errors. When p_{like} is evaluated at the observed values η^{obs} and considered as a function of the model parameters x, it becomes the likelihood function $\pi(x;\eta^{\text{obs}})$ [46]. In order to construct a likelihood function, an error model should be defined first. Here, the error model is defined as:

$$\eta_i^{\text{obs}} = \eta_i(x) + \epsilon_i \, , \tag{4}$$

where ϵ_i refers to the experimental error of the measurement i, consequently assuming an exact model. Unlike several studies in the past [46, 47], the use of a hyper-parameter to identify model errorspast is not used here. Since the focus here is on the development of a calibrated chemical mechanism for use in a deterministic manner, such a model-error approach [46, 47] is not suitable. If data can be obtained with zero errors, the assumption states that the parameters could be fitted perfectly and the model could thus predict experiment exactly. The errors in experiments are assumed to be independent, normally distributed random variables with $\epsilon_i \sim \mathcal{N}_{\mathrm{i}}(0, \sigma_i^2)$. Thus, the likelihood function with n experiments can be formulated as:

$$\pi(x; \eta^{\mathrm{obs}}) = \frac{1}{\prod_{i=1}^{n} (2\pi\sigma_i^2)^{\frac{1}{2}}} \exp\left[-\frac{1}{2}\sum_{i=1}^{n} \frac{1}{\sigma_i^2}\left(\eta_i^{\mathrm{obs}} - \eta_i(x)\right)^2\right] . \tag{5}$$

As mentioned by Braman et al. [46], the Bayesian approach provides a naturally self-consistent process for learning based on available information. The posteriors from one optimization can be further used as the priors for subsequent calibrations, once more experimental measurements become available.

2.2.2. Computational details

In the present study, the Bayesian approach is implemented with the statistical QUESO library [48]. For each experimental condition included in the optimization process, a sensitivity analysis of the rate rules is carried out. The rate rules with the highest sensitivities (>2%) in the range of the experimental conditions are selected automatically as active parameters. The uncertainties of the rate rules are assumed to be temperature-independent according to Ref. [27], and thus only the Arrhenius pre-exponential factors

A are considered as calibration objectives. The current state of knowledge about the rate rules is represented by uniformly distributed PDFs bounded by the lower and upper limits of the pre-exponential factors. The prior pre-exponential factors and their uncertainty limits used here are shown in Table 2. Note that the prior selection affects the posterior distributions, as quantified in Ref. [46]. While the bounds of the uniform prior limit the posterior distribution, the Gaussian prior does not posit a bound on the parameter [46], which is useful if this parameter information is not available a priori. However, for an underconstrained calibration case, the application of Gaussian priors can shift the posteriors to a domain, which is not covered by the existing rate data.

The likelihood function is specified according to Eq. (5). The posterior PDFs are estimated by solving Eq. (2) with the Markov Chain Monte Carlo (MCMC) sampling algorithm [46, 49, 50]. In the present study, the mean values of the posterior PDFs are defined as the pre-exponential factors of the optimized rate rules and further incorporated in chemical mechanisms. It is also found that the performance of the mechanism developed with the mean values of the posterior PDFs is almost identical with the one based on the peak values of PDFs. Due to the large number of samples, the model predictions are calculated through the response surface technique [35], which relates the model parameters to the prediction targets in form of a second order polynomial. The coefficients in the response surface are calculated by the sensitivity analysis based (SAB) method [51], and the required simulations are performed using the appropriate reactor modules in the FlameMaster [52] code, with the source code available at www.itv.rwth-

aachen.de/downloads/flamemaster/.

3. Mechanism development

A newly developed kinetic mechanism for C_7–C_{11} normal alkanes is presented in this section. The chemical mechanism for *n*-alkanes and 2-methylalkanes [8] served as the starting point in the development procedure. This mechanism [8] was updated according to the recent work by Bugler et al. [27]. Subsequently, the mechanism was reduced to a skeletal level in order to enable the optimization within a reasonable computational time.

3.1. Mechanism modification

Sarathy et al. [8] presented a detailed chemical kinetic mechanism (referred to as "LLNL" mechanism) for the oxidation of singly methylated isoalkanes (i.e., 2-methylalkanes) ranging from C_7–C_{20}, which also included an updated version of the previously published model for C_8–C_{16} *n*-alkanes [7]. While the model predicted the oxidation of normal alkanes with a moderate accuracy, discrepancies were observed between experiments and simulations, especially for ignition delay times [8]. Recently, Bugler et al. [27] investigated the auto-ignition of three pentane isomers and improved the general understanding of low temperature oxidation kinetics. They stated that errors from both thermochemistry and rate constant assignments compensated each other in past models [5–7]. Based on a thorough literature review, they revised rate rules for important low temperature reaction classes. Species thermochemical data were estimated with refined group additivity values from Burke et al. [53]. Moreover, alternative isomerization pathways of O_2QOOH radicals were proposed. In contrast to the conventional isomerization, in

which an H atom is abstracted from the carbon site bonded to the hydroperoxy group, the H atom can now also be released from a normal C-H bond via 5, 6, 7, and 8-membered transition state rings. Due to the lower energy barriers, the channels with six-membered transition state rings are dominant. All these modifications [27] were incorporated into the LLNL mechanism in this study.

The update was performed in three steps: (a) The thermochemical data of species involved in the oxidation of C_7–C_{11} alkanes were first recalculated using the group additivity method [54] with the revised group values [53] in the THERM code [55]. (b) Following this, the rate rules in the LLNL mechanism were replaced by the rate rules recommended in Ref. [27]. For H-atom abstractions from the fuel by OH radicals, Sivaramakrishnan and Michael [56] reported different barrier heights at various carbon sites and experimentally investigated the site specific rate rules for these reactions in a rigorous manner. These accurate site specific rate rules [56] were also incorporated into the mechanism. (c) Finally, the alternative reaction pathways of O_2QOOH producing di-hydroperoxy alkyl radicals $P(OOH)_2$ were included in the mechanism. Only the channels with six-membered transition state rings were taken into account due to their lower energy barriers and expected dominance [27]. Two consumption channels were proposed for $P(OOH)_2$ radicals. The $P(OOH)_2$ radical can either go through a β-scission to form an olefin and a hydroperoxyl radical or decomposes to produce a cyclic ether and an OH radical. The cyclization of $P(OOH)_2$ radicals takes place at O_2QOOH to $P(OOH)_2$ isomerization site. For the O_2QOOH species having conventional ketohydroperoxide formation pathways via 6-membered transition state ring,

alternative pathways were not considered in the mechanism. The modified mechanism consists of 1692 species among 11015 reactions (forward and backward counted separately). The effects of these revisions are demonstrated in the following example in terms of the ignition delay times of n-decane.

Figure 1 contains the ignition delay times of stoichiometric n-decane/air mixtures at 12 atm. Over the entire temperature range, the LLNL model [8] predicts the ignition delay times with decent accuracy. At intermediate temperatures, it underpredicts the data with a factor of around 3. After the revision of the thermochemistry, the computed ignition delays increase significantly at intermediate temperatures. With the further update of the rate rules, the numerical results decrease in the low to intermediate temperature range. Compared with these two alterations, the impact of alternative pathways of O_2QOOH radicals on ignition is smaller but not negligible. Normally, an O_2QOOH radical undergoes an internal H-atom migration to release an OH radical and forms a ketohydroperoxide. The ketohydroperoxide decomposes to produce a second OH radical, which results in a chain branching in the low temperature range. Alternatively, the O_2QOOH radical can now isomerize to form a di-hydroperoxy alkyl radical. While this isomerization step does not directly release an OH radical, the consumption pathways of $P(OOH)_2$ can produce two OH radicals. Again, a chain branching pathway is established at low temperatures. Compared with the conventional isomerization via five- or eight-membered transition state rings, the alternative channel is based on a rapid six-membered ring H-atom migration and thus becomes favorable. As shown in Fig. 1, this alternative isomerization enhances the fuel ignition propensity at low to intermediate temperatures.

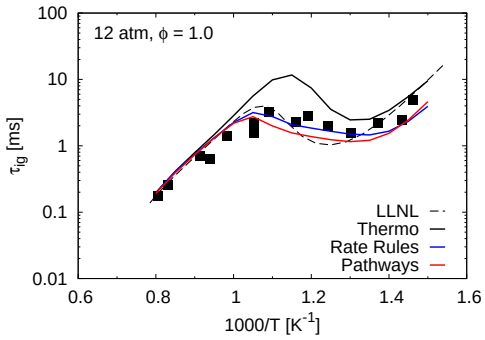

Figure 1: Ignition delay times of n-decane/air mixtures. Symbols denote experimental measurements [58]. Dashed line shows the results using the LLNL model [8]. Black, blue, and red solid lines show the results for the model after revision steps (a), (b), and (c), respectively.

The effects of these three modifications on the auto-ignition of n-decane are consistent with those reported for pentane isomers [27] and those observed for the other normal alkanes studied in this work. The cases of n-octane and n-nonane are shown in the Supplementary material. In comparison with the previous LLNL mechanism, the modified mechanism predicts the ignition delay times at low and intermediate temperatures with slightly improved accuracy. The slope of the measured ignition delay times in the intermediate temperature range is well reproduced by the updated mechanism. The developed kinetic knowledge from Bugler et al. [27] demonstrates here the capability to improve the model prediction precision. Nevertheless, differences still exist between the updated mechanism and the experimental data, which motivates the further calibration of rate rules.

3.2. Mechanism reduction

While the application of the response surface technique [35, 51] contributes to a significant reduction in the computational cost of Bayesian analysis, a large amount of numerical calculations are still required to generate the response surface. In order to minimize this computational effort, the updated mechanism was reduced to a skeletal level using a multi-stage reduction strategy proposed by Pepiot-Desjardins and Pitsch [57]. The directed relation graph method with error propagation (DRGEP) [57] selects the important reaction channels based on the evaluation of species production and consumption rates. The reduction procedure involved the elimination of species and reactions. The lumping of chemical species presented in Ref. [57] was excluded, as the isomerization of intermediates plays a major role in fuel oxidation and thus the involved rate coefficients are of particular importance for model predictions. The targets in the reduction include concentrations of various major species for varying initial pressures, temperatures, and equivalence ratios. Very small error tolerances were specified for the deviations of targets between the skeletal and the detailed mechanisms. This reduction process, and specifically the error propagation algorithm, ensure that only those species and reactions are removed, which have a minimal impact on the chemistry of the reduction targets. Ignition delay times are not direct targets in the reduction, but are inherently preserved by correctly predicting the chemistry of the target species. The reduced model is composed of 624 species with 2727 reactions (forward and backward counted separately). The computed ignition delay times of n-decane using the detailed and the reduced mechanisms are compared in Fig. 2. For the experimental conditions

studied, the differences between the detailed and the reduced mechanisms are marginal. Good agreement between both mechanisms is also observed for the auto-ignition of *n*-heptane, *n*-octane, *n*-nonane, and *n*-undecane.

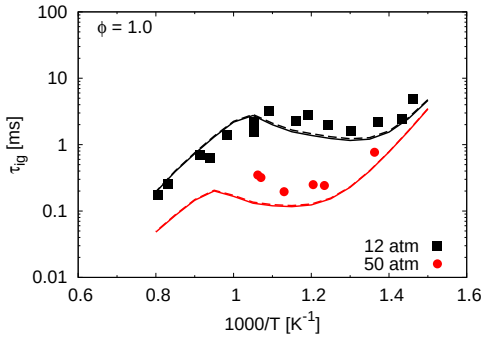

Figure 2: Ignition delay times of *n*-decane/air mixtures. Symbols denote experimental measurements [58]. Solid lines show the results for the model developed in Section 3.1, and dashed lines show the results for the reduced model.

4. Rate rule calibration

In this section, the training of the rate rules is described. A large number of experimental data sets for *n*-heptane, *n*-octane, *n*-nonane, *n*-decane, and *n*-undecane were taken into consideration. Using the Bayesian method described in Section 2, the rate rules used in the reduced chemical mechanism for C_7–C_{11} *n*-alkanes were calibrated automatically for the given data sets for different fuels.

4.1. Experimental database

An overview of the experimental data sets used in the Bayesian analysis is shown in Table 1. Experimental ignition delay times were reported

for n-heptane [59, 60], n-octane [8], and n-decane [58, 61] for a variety of conditions covering the entire range of temperatures. For n-nonane and n-undecane, measurements were solely performed for diluted mixtures at high temperatures [62, 63]. Overall, 198 experimental data points were taken into account in the optimization process.

Campbell et al. [59] stated an uncertainty of $\pm 25\%$ for their n-heptane ignition data. The uncertainties in the ignition delay times were mainly attributed to uncertainties in reflected shock pressures and temperatures, mixture compositions, and signal determinations [59]. An uncertainty of $\pm 10\%$ was estimated by Rotavera and Petersen [62] for the ignition delay times of n-nonane and n-undecane. A pressure uncertainty of ± 2 bar was reported in Ref. [60] for the auto-ignition of n-heptane/air mixtures at a pressure of 40 bar. This pressure variation was related to a standard deviation of approximately 10% in ignition delays. These reported uncertainties [59, 60, 62] were used in the calibration for the corresponding experiments. Uncertainty estimates were missing in several studies [8, 58, 61]. For these measurements, an uncertainty of $\pm 10\%$ was assumed. Pressure increase due to shock attenuation was observed in the shock tube measurements by Rotavera and Petersen [62] and Sarathy et al. [8]. It was found [8] that the effect of pressure increase becomes important only at very low temperatures. Therefore, the measurements for n-octane [8] at very low temperatures were excluded from the optimization.

The database excludes the ignition delay times from rapid compression machines (RCM), as common 0D RCM simulation approaches utilizing pressure traces of non-reactive mixtures are associated with a maximum predic-

tion deviation of 30% [68]. The experimental burning velocities of C_7–C_{11} alkanes were included in the calibration process. However, these targets were automatically exempted from the optimization after sensitivity analyses, as their prediction are found to be negligibly influenced by the rate rules. The prediction of flame speeds depends solely on the reactions involved in the base mechanism [10]. Also, the prediction of small hydrocarbon species profiles typically measured in flow and jet stirred reactors is highly sensitive to the reactions involving small species [43, 69]. Therefore, this study focuses on fuel auto-ignition in shock tubes, which is mainly influenced by the fuel specific reactions and can be accurately reproduced by common 0D simulations.

Note that two data sets were reported by Campbell et al. [59] for *n*-heptane at identical conditions. The first data set was measured in a conventional shock tube, where the auto-ignition takes place nominally at a constant volume. The second set was measured with the novel Constrained Reaction Volume (CRV) technique under constant pressure conditions. It was found in this study that the experimental data set measured with the novel CRV technique was inconsistent with other experimental data. Therefore, this data set was excluded from the automatic calibration. A more detailed discussion is presented in Section 4.4.

4.2. Model calibration and uncertainty quantification

The reduced mechanism for the oxidation of C_7–C_{11} normal alkanes was subjected to the automatic optimization. The sensitive rate rules were chosen as active parameters. For the given experimental data sets, the joint posterior PDFs of the rate rules were determined based on the Bayesian theorem. By means of a Monte Carlo sampling algorithm, the uncertainties of the rate

Fuel	Pressure [bar]	Equivalence Ratio [-]	No. Data	Ref.
n-Heptane	6.5	0.75 (diluted)	22	[59]
	13.5	0.5, 1.0, 2.0	49	[60]
	42.0	0.5, 1.0, 2.0	22	[60]
n-Octane	20.3	0.5, 1.0, 1.5	59	[8]
n-Nonane	1.5	1.0 (diluted)	10	[62, 63]
n-Decane	12.2	1.0	14	[58]
	50.7	1.0	6	[58]
	81.1	0.5, 1.0	10	[61]
n-Undecane	1.5	1.0 (diluted)	6	[62]

Table 1: Experimental database.

rules were propagated into the simulation results. In this way, the model prediction uncertainties were quantified.

The ignition delay times computed with the optimized mechanism for normal alkanes are presented in Figs. 3–7 in comparison with measurements. It is shown that the model with the optimized common rate rules yields a very good agreement with experiments. Compared with the mechanism developed in Section 3, which incorporates the up-to-date kinetic knowledge, the optimized model predicts the ignition delay times with improved accuracy over a wide variety of initial conditions, especially at intermediate temperatures.

Note that ignition delay times are generally underpredicted by the unoptimized model in the low and intermediate temperature ranges. A strong deviation is seen for the case of *n*-heptane, which indicates that the unoptimized set of rate rules is less suitable for this fuel, while relatively more

appropriate for larger species. In addition, the prior set predicts lean auto-ignition with higher accuracy than auto-ignition at rich conditions. These observations lend further support to the proposed methodology, which calibrates rate rules across a family of fuels rather than for each fuel individually and includes a large number of experimental data covering a wide range of initial conditions.

The optimized model is validated in the Supplementary material against the species concentration measurements for n-heptane in jet stirred reactors [64, 65] and for n-octane [66] and n-decane [67] in flow reactors, which were not part of the optimization. Nevertheless, the model again appears satisfactory.

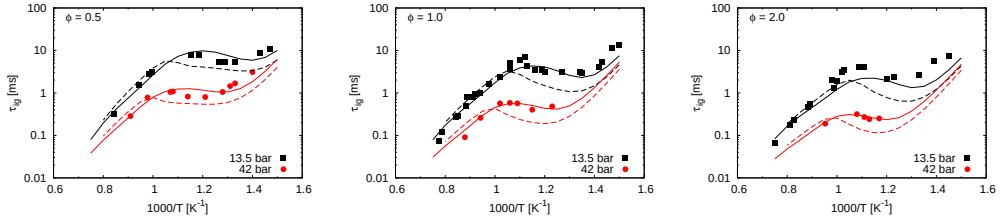

(a) $\phi = 0.5$ (b) $\phi = 1.0$ (c) $\phi = 2.0$

Figure 3: Ignition delay times of n-heptane/air mixtures. Symbols denote experimental measurements [60]. Solid lines show the numerical results for the present optimized model, and dashed lines show the results for the unoptimized model.

4.3. Rate rules

57 important rate rules from 21 reaction classes were calibrated automatically. The sensitive reaction classes at high temperatures contain the fuel decomposition (C1), the H-abstraction from fuel (C2), the decomposition (C3) and the isomerization (C4) of fuel radicals, and the decomposition of

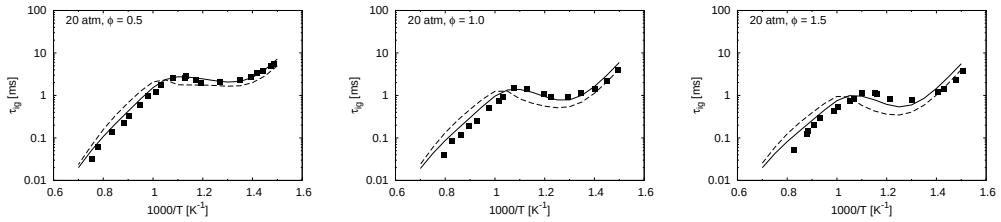

(a) $\phi = 0.5$ (b) $\phi = 1.0$ (c) $\phi = 1.5$

Figure 4: Ignition delay times of n-octane/air mixtures. Symbols denote experimental measurements [8]. Solid lines show the numerical results for the present optimized model, and dashed lines show the results for the unoptimized model.

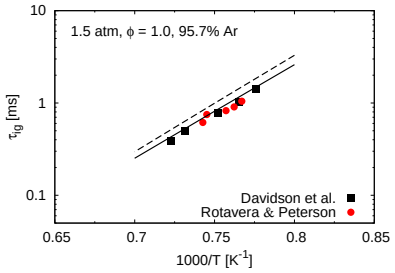

Figure 5: Ignition delay times of n-nonane/oxygen/argon mixtures. Symbols denote experimental measurements [62, 63]. Solid line shows the numerical results for the present optimized model, and dashed line shows the results for the unoptimized model.

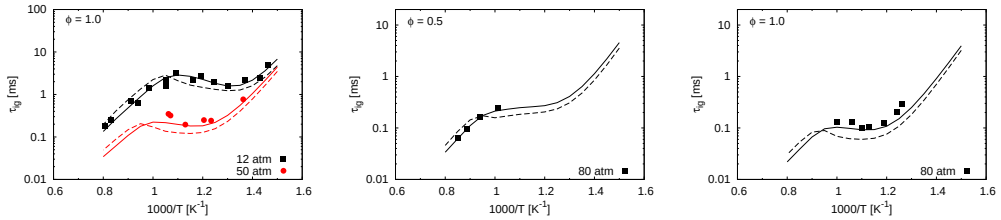

(a) 12 and 50 atm, $\phi = 1.0$ (b) 80 atm, $\phi = 0.5$ (c) 80 atm, $\phi = 1.0$

Figure 6: Ignition delay times of n-decane/air mixtures. Symbols denote experimental measurements [58, 61]. Solid lines show the numerical results for the present optimized model, and dashed lines show the results for the unoptimized model.

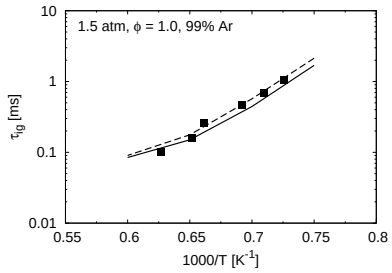

Figure 7: Ignition delay times of *n*-undecane/oxygen/argon mixtures. Symbols denote experimental measurements by Rotavera and Petersen [62]. Solid line shows the numerical results for the present optimized model, and dashed line shows the results for the unoptimized model.

alkenyl radicals (C8) as well as alkene species (C9). The reaction classes 11, 15, 26, 27, and 28 complete the low temperature chain branching pathway and are dominant at low to intermediate temperatures. Several additional reaction classes are also rate-controlling at low to intermediate temperatures. In reaction class 13, alkyl radicals react with HO_2 to yield an OH, leading to chain propagation. The concerted elimination of RO_2 radicals occurs via 5-membered transition state rings. Besides the oxidation pathway, three decomposition channels of QOOH radicals (C23, C24, and C25) also play a major role at relevant conditions. All these reaction steps compete with the chain branching pathway and thus prolong auto-ignition. The alternative isomerization of O_2QOOH is found to be sensitive as well. The promoting effect of this reaction class on ignition was shown in Section 3. Note that only the rate rules for primary and secondary carbon sites are considered in the present work, as *n*-alkanes do not contain tertiary carbon sites.

The calibrated rate rules are summarized in Table 2 along with the orig-

inal values and their uncertainties. Uncertainty limits were reported for several low temperature reaction classes (e. g. Class 23: QOOH = cyclic + OH) by Bugler et al. [27] and were taken into account in this work. The site specific rate rules for the H-abstraction from the fuel by OH radical proposed by Sivaramakrishnan and Michael [56] predict the total rate constant for *n*-heptane + OH within an uncertainty of 10%. This corresponds to an uncertainty estimate of 41.9% for the rate rule at the P_1 carbon site at a temperature of 1000 K, if the error in the overall rate is caused exclusively by this rate rule. Similarly, uncertainties of the rate rules at S_{01}, S_{11}, and $S_{11'}$ sites are deduced as 29.1%, 39.4%, and 60.8%, respectively. For the rate rules without uncertainty estimates in the literature, an uncertainty factor of four is defined, as large uncertainties can be expected [40].

It is found that most rate rules are altered strongly after the calibration. One reason for this is the form of the prior PDF of the rate rule values. A uniform distribution indicates a minor confidence of the prior rate estimation. All values between the lower and upper uncertainty limits are equally likely.

In the applied Bayesian framework, the posterior joint and marginal PDFs of parameters and model predictions can be constructed from the sampling results. Standard deviations (σ) of marginal parameter PDFs are given in Table 2 as the uncertainties of rate rules. A 95% confidence interval of distributions is employed to indicate the model prediction uncertainties [46]. The large number of measurements and their small uncertainties strongly constrain the uncertainties of rate rules and thus also the model prediction uncertainties. For the most studied cases, the 95% confidence interval of prediction distributions corresponds to an uncertainty in the range of 0.5–

5%. The prediction uncertainties of ignition delay times for C_7–C_{11} normal alkanes are shown in the Supplementary material.

With the aid of the UQ framework, the knowledge about rate rules is updated by extracting information from experimental data of *n*-heptane, *n*-octane, *n*-nonane, *n*-decane, and *n*-undecane. As expected, these optimized common rate rules demonstrate their capability to improve the model performance for the fuels considered in the calibration.

4.4. Data consistency

While most experiments are well reproduced by the optimized model, the constant pressure auto-ignition of *n*-heptane at a pressure of 6.5 atm [59] appears as an outlier. In Fig. 8, the unoptimized model predicts the total ignition delay times measured with the novel CRV technique reasonably well, but substantially underpredicts the first stage ignition data. After the model optimization, the computed first stage ignition delay times appear satisfactory for the conditions studied, while the entire ignition delays are now overpredicted. To gain more insight into this, the prior 2D joint PDFs of several prediction targets are presented in Fig. 9 in form of kernel density estimation (KDE). Details of these targets are summarized in Table 3 as well as in Figs. 8 and 10. A Monte Carlo sampling algorithm is used to determine the error distribution of prediction targets. Random samples are generated to represent the rate parameters according to their specified prior PDFs. For each sample of the parameter set, targets are calculated for all conditions of interest. This leads to an ensemble of prediction values that can be used to estimate the joint distribution of prediction targets. The joint PDF explores how changing the value of a rate parameter requires other parameters

Class	Rate rules	Uncertainties (lower, upper)	A_0 [cm^3,s,mol,K]	A^* [cm^3,s,mol,K]	n [-]	E [cal/mol]	σ^*
C1	Fuel decomposition → H and alkyl radical	[4.0, 4.0]	1.000×10^{14}	4.048×10^{13}	0.00	0	0.0395
C1	Fuel decomposition → CH_3 and alkyl radical	[4.0, 4.0]	1.000×10^{13}	4.454×10^{12}	0.00	0	0.0297
C1	Fuel decomposition → alkyl radicals	[4.0, 4.0]	8.000×10^{12}	1.774×10^{13}	0.00	0	0.0783
C2	H-atom abstraction from the fuel by H (primary carbon sites)	[4.0, 4.0]	2.220×10^{05}	2.922×10^{05}	2.54	6756	0.0675
C2	H-atom abstraction from the fuel by H (secondary carbon sites)	[4.0, 4.0]	6.500×10^{05}	1.635×10^{05}	2.40	4471	0.0339
C2	H-atom abstraction from the fuel by OH (P_1)	[1.4, 1.4]	4.553×10^{06}	6.422×10^{06}	1.81	868	0.0129
C2	H-atom abstraction from the fuel by OH (S_{01})	[1.3, 1.3]	3.528×10^{09}	2.780×10^{09}	0.94	505	0.0231
C2	H-atom abstraction from the fuel by OH (S_{11})	[1.4, 1.4]	2.860×10^{06}	3.950×10^{06}	1.81	-1016	0.0125
C2	H-atom abstraction from the fuel by OH ($S_{11'}$)	[1.6, 1.6]	2.810×10^{11}	1.761×10^{11}	0.32	847	0.0202
C2	H-atom abstraction from the fuel by HO_2 (primary carbon sites)	[4.0, 4.0]	6.800×10^{00}	6.627×10^{00}	3.59	17160	0.0831
C2	H-atom abstraction from the fuel by HO_2 (secondary carbon sites)	[4.0, 4.0]	3.160×10^{01}	1.258×10^{02}	3.37	13720	0.0410
C2	H-atom abstraction from the fuel by CH_3 (secondary carbon sites)	[4.0, 4.0]	7.550×10^{-01}	3.718×10^{-01}	3.46	5481	0.0287
C2	H-atom abstraction from the fuel by O_2 (primary carbon sites)	[4.0, 4.0]	1.000×10^{13}	5.942×10^{12}	0.00	52290	0.0477
C2	H-atom abstraction from the fuel by O_2 (secondary carbon sites)	[4.0, 4.0]	1.000×10^{13}	1.338×10^{13}	0.00	49640	0.0585
C2	H-atom abstraction from the fuel by C_2H_5 (secondary carbon sites)	[4.0, 4.0]	2.500×10^{10}	1.279×10^{10}	0.00	10400	0.0637
C2	H-atom abstraction from the fuel by CH_3O_2 (secondary carbon sites)	[4.0, 4.0]	5.090×10^{00}	2.442×10^{00}	3.58	14810	0.0695
C3	Alkyl radical (R) decomposition → alkene and H (primary carbon sites)	[4.0, 4.0]	4.240×10^{11}	2.220×10^{11}	0.51	1230	0.0474
C3	Alkyl radical (R) decomposition → alkene and H (secondary carbon sites)	[4.0, 4.0]	2.500×10^{11}	1.636×10^{11}	0.51	2620	0.0550
C3	Alkyl radical (R) decomposition → CH_3 and alkene	[4.0, 4.0]	9.550×10^{09}	2.651×10^{09}	1.08	29388	0.1330
C3	Alkyl radical (R) decomposition → C_2H_4 and alkyl radical	[4.0, 4.0]	9.120×10^{11}	3.579×10^{12}	0.31	27238	0.0120
C3	Alkyl radical (R) decomposition → alkyl radical and alkene	[4.0, 4.0]	6.000×10^{11}	1.029×10^{12}	0.50	27650	0.0464
C4	Alkyl radical (R) isomerization (5 member ring, secondary to primary carbon sites)	[4.0, 4.0]	3.460×10^{00}	1.401×10^{00}	3.20	16558	0.0190
C4	Alkyl radical (R) isomerization (5 member ring, secondary to secondary carbon sites)	[4.0, 4.0]	7.100×10^{-01}	1.734×10^{00}	3.32	16140	0.0532
C4	Alkyl radical (R) isomerization (6 member ring, secondary to primary carbon sites)	[4.0, 4.0]	9.100×10^{01}	3.295×10^{02}	2.55	10960	0.0217
C4	Alkyl radical (R) isomerization (6 member ring, secondary to secondary carbon sites)	[4.0, 4.0]	9.310×10^{-01}	1.457×10^{00}	3.27	13200	0.0458
C4	Alkyl radical (R) isomerization (7 member ring, secondary to primary carbon sites)	[4.0, 4.0]	1.480×10^{00}	1.941×10^{00}	3.08	11020	0.0401
C5	H-atom abstraction from alkene by H	[4.0, 4.0]	1.040×10^{07}	5.019×10^{06}	2.400	4471	0.0245
C5	H-atom abstraction from alkene by OH	[4.0, 4.0]	3.740×10^{08}	2.406×10^{08}	1.610	-35	0.0751
C5	H-atom abstraction from alkene by HO_2	[4.0, 4.0]	5.060×10^{02}	2.347×10^{02}	3.370	13720	0.0573
C8	Alkenyl radical decomposition → alkene and allyl (C_3H_5)	[4.0, 4.0]	2.500×10^{13}	1.222×10^{13}	0.00	25000	0.0226
C9	Alkene decomposition	[4.0, 4.0]	2.500×10^{16}	5.344×10^{16}	0.00	71000	0.0309
C11	Addition of O_2 to alkyl radicals (R) (primary carbon sites)	[2.2, 1.7]	1.301×10^{11}	8.898×10^{10}	0.23	-1580	0.0252
C11	Addition of O_2 to alkyl radicals (R) (secondary carbon sites)	[1.7, 2.1]	1.507×10^{15}	1.039×10^{15}	-0.92	-130	0.0238
C13	R + HO_2 → RO + OH	[4.0, 4.0]	7.000×10^{12}	1.227×10^{13}	0.00	-1000	0.0442
C15	Alkyl peroxy radical isomerization (5 member ring, secondary carbon sites)	[3.1, 4.2]	2.327×10^{07}	1.506×10^{07}	1.40	28660	0.0839
C15	Alkyl peroxy radical isomerization (6 member ring, primary carbon sites)	[2.7, 2.5]	5.869×10^{08}	5.680×10^{08}	0.78	21850	0.0446
C15	Alkyl peroxy radical isomerization (6 member ring, secondary carbon sites)	[2.3, 2.2]	8.204×10^{10}	5.010×10^{10}	0.13	19470	0.0352
C15	Alkyl peroxy radical isomerization (7 member ring, secondary carbon sites)	[2.3, 1.6]	7.054×10^{08}	3.079×10^{08}	1.00	21070	0.0142
C15	Alkyl peroxy radical isomerization (8 member ring, secondar carbon sites)	[3.6, 1.4]	1.143×10^{10}	1.357×10^{10}	0.04	19780	0.0540
C16	Concerted eliminations (RO_2 → alkene + HO_2)	[2.2, 2.8]	2.885×10^{09}	6.650×10^{09}	0.93	29800	0.0201
C23	QOOH → cyclic ether + OH (3 member ring)	[3.3, 3.4]	2.282×10^{08}	1.389×10^{08}	1.29	9890	0.0354
C23	QOOH → cyclic ether + OH (4 member ring)	[11.1, 35.8]	4.579×10^{15}	6.130×10^{15}	-1.08	18440	0.0450
C23	QOOH → cyclic ether + OH (5 member ring)	[6.2, 7.4]	3.502×10^{10}	6.974×10^{09}	0.10	9330	0.1120
C23	QOOH → cyclic ether + OH (6 member ring)	[4.0, 4.3]	3.553×10^{07}	9.621×10^{07}	0.69	10970	0.0348
C24	QOOH → alkene + HO_2	[3.3, 2.4]	1.829×10^{10}	1.016×10^{10}	0.79	15100	0.0539
C25	QOOH → β-Scission products	[6.0, 8.5]	5.819×10^{05}	1.319×10^{06}	2.40	22790	0.0414
C26	Addition of O_2 to QOOH (primary carbon sites)	[4.0, 4.0]	6.505×10^{10}	1.034×10^{11}	0.23	-1580	0.0974
C26	Addition of O_2 to QOOH (secondary carbon sites)	[4.0, 4.0]	7.535×10^{14}	4.449×10^{14}	-0.92	-130	0.0083
C27	Isomerization of O_2QOOH (6 member ring, primary OOH and secondary OO sites)	[4.0, 4.0]	5.489×10^{03}	2.628×10^{03}	2.40	19900	0.0494
C27	Isomerization of O_2QOOH (6 member ring, secondary OOH and secondary OO sites)	[4.0, 4.0]	1.754×10^{02}	4.471×10^{02}	3.10	17500	0.0326
C27	Isomerization of O_2QOOH (7 member ring, secondary OOH and secondary OO sites)	[4.0, 4.0]	2.536×10^{02}	1.184×10^{02}	2.60	16200	0.0493
C27	Isomerization of O_2QOOH (8 member ring, secondary OOH and primary OO sites)	[4.0, 4.0]	1.995×10^{03}	7.775×10^{03}	1.90	14900	0.0321
C28	Decomposition of carbonylhydroperoxide	[4.0, 4.0]	1.000×10^{16}	6.065×10^{15}	0.00	3900	0.0359
C29	Cyclic ether reactions with OH	[4.0, 4.0]	2.500×10^{12}	1.045×10^{12}	0.00	0	0.0492
C29	Cyclic ether reactions with HO_2	[4.0, 4.0]	5.000×10^{12}	1.988×10^{13}	0.00	17700	0.0113
C30	H-atom abstraction from aldehyde by OH	[4.0, 4.0]	2.690×10^{10}	3.582×10^{10}	0.76	-340	0.0491
C31	Alternative isomerization of O_2QOOH (6 member ring, secondary carbon sites)	[4.0, 4.0]	8.204×10^{10}	1.233×10^{11}	0.13	19470	0.0620

Table 2: Unoptimized and optimized rate rules; per H-atom basis. The lower and upper limits are the prior uncertainty limits. σ^* denote the standard deviation of optimized rate rules.

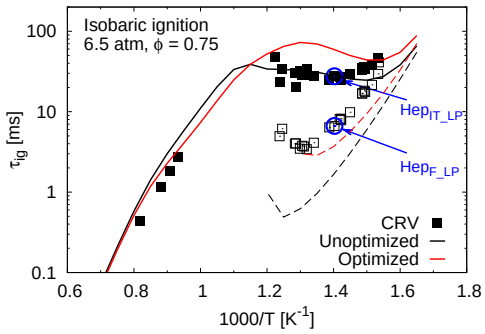

Figure 8: Ignition delay times of n-heptane/15%O_2/5%CO_2/Ar mixtures. Solid and open symbols denote the experimental total and first stage ignition delay times, respectively [59]. Solid and dashed lines show the numerical results for the total and first stage ignition delay times, respectively. Details on the circled points are provided in the main text.

to change in order to still yield acceptable predictions. If, for example, the joint PDF covers a wide area (e. g. as shown in Fig. 9(a)), then both predicted quantities can vary in their uncertainty limits independently. In other words, within the specified or determined uncertainties of the rate coefficients, there are probable combinations of rate parameters for independent variations of predicted ignition delays. If, however, the domain of the joint PDF covers a narrow region (e. g. in Fig. 9(b)), the change of rate parameters within the uncertainties would always lead to joint change in both predicted ignition delays.

It is interesting to observe in Fig. 9(a) that the first stage ignition delay times (Case $\mathrm{Hep_{F\_LP}}$) and the total ignition delay times (Case $\mathrm{Hep_{IT\_LP}}$) for n-heptane at 6.5 atm and 753 K are only weakly correlated. This allows for the possibility of increasing the first stage ignition delay time and simultaneously leaving the total ignition delay time unchanged in the model calibration.

Case	Fuel	Condition	Ignition delay
$\text{Hep}_{\text{IT\_HP}}$	n-heptane	740 K, 13.5 bar, $\phi = 1.0$	Total
$\text{Hep}_{\text{LT\_HP}}$	n-heptane	667 K, 13.5 bar, $\phi = 1.0$	Total
$\text{Hep}_{\text{IT\_LP}}$	n-heptane	713 K, 6.5 atm, ϕ= 0.75	Total
$\text{Hep}_{\text{F\_LP}}$	n-heptane	713 K, 6.5 atm, $\phi = 0.75$	First stage
$\text{Dec}_{\text{LT\_HP}}$	n-decane	734 K, 50.0 atm, $\phi = 1.0$	Total

Table 3: Calibration cases.

However, this is not observed after the calibration. The reason here lies in the strong correlation of Case $\text{Hep}_{\text{IT\_LP}}$ with cases at intermediate temperatures, e. g. Case $\text{Hep}_{\text{IT\_HP}}$, as demonstrated in Fig. 9(b). In Fig. 10, an increased ignition delay time is observed for Case $\text{Hep}_{\text{IT\_HP}}$ after the calibration. Due to the strong correlation between these two cases, the total ignition delay time of Case $\text{Hep}_{\text{IT\_LP}}$ is inevitably increased.

Case $\text{Hep}_{\text{LT\_HP}}$ describes the auto-ignition of n-heptane at 667 K and 13.5 bar. At this condition, a large temperature rise is observed after the first stage auto-ignition, which enables a rapid consumption of ketohydroperoxide and results in a very short second stage induction. The first stage ignition delay time is thus almost identical to the total ignition delay time. As shown in Fig. 9, this case is strongly correlated with Case $\text{Hep}_{\text{F\_LP}}$, as the ignition delay times at both conditions are mainly affected by the low temperature oxidation chemistry. Case $\text{Dec}_{\text{LT\_HP}}$ is also connected with Case $\text{Hep}_{\text{F\_LP}}$, even though Case $\text{Dec}_{\text{LT\_HP}}$ presents the oxidation of n-decane at a very high pressure of 50 atm. As the initial temperature of Case $\text{Dec}_{\text{LT\_HP}}$ is relatively low, the prediction of the ignition delay time is again only sensitive to low

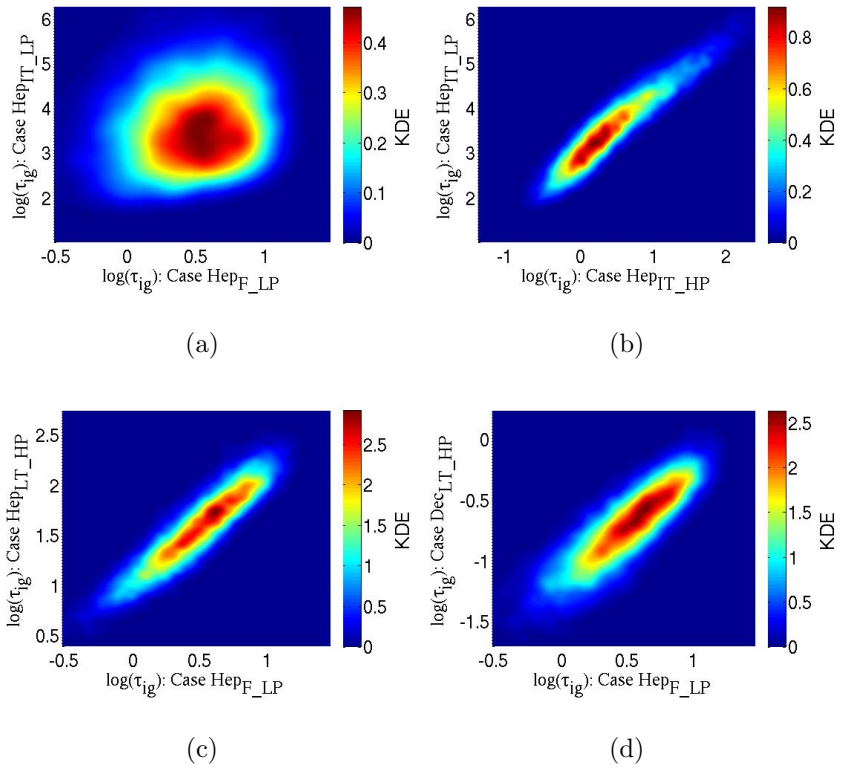

Figure 9: 2D prior joint PDFs of prediction targets. The log values of these prediction targets are presented.

temperature pathways. Moreover, common rate rules are used here for both *n*-heptane and *n*-decane. Due to these two facts, a strong correlation is established between Case $\mathrm{Dec}_{\mathrm{LT\_HP}}$ and Case $\mathrm{Hep}_{\mathrm{F\_LP}}$.

4.5. Base chemistry

In the current model development procedure, a well-studied $\mathrm{C_0}$–$\mathrm{C_4}$ kinetic mechanism is taken as the base mechanism to describe the oxidation of intermediate species [8]. Its accuracy is of particular importance for the prediction of species profiles and burning velocities. Therefore, the effect of the

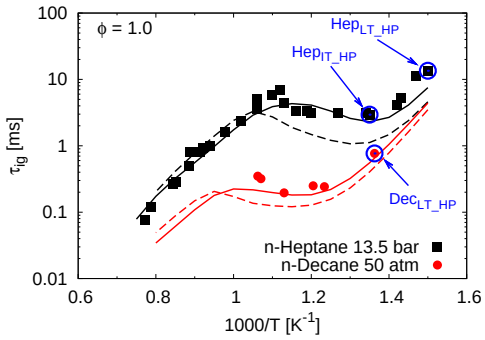

Figure 10: Ignition delay times of n-heptane/air and n-decane/air mixtures. Solid symbols denote experimental measurements [58, 60]. Solid lines show the numerical results for the present optimized model, and dashed lines show the results for the unoptimized model. Details on the circled points are provided in the main text.

base chemistry on the application and calibration of rate rules is evaluated in the following.

The base mechanism in the optimized model was replaced by the one from Narayanaswamy et al. [43] without alterations in the fuel specific chemistry. The numerical results of n-octane ignition delay times using that base mechanism (referred to as "Narayanaswamy") are shown in Fig. 11, along with those computed with the optimized mechanism. For all conditions numerically studied, both models yield almost identical results. The calibration of rate rules is hence, at least in this example, independent of the base chemistry, which has often been assumed in past studies [5–11]. Regardless of the chosen base mechanism, identical reaction classes and rate rules have typically been employed to derive the fuel specific chemistry in various mechanisms. Nevertheless, it should be mentioned again that, even though the calibration and application of rate rules are not sensitive to the base chemistry, the

choice of the base mechanism is still of great importance. For example, the prediction of flame speeds depends solely on the reactions involved in the base mechanism [10].

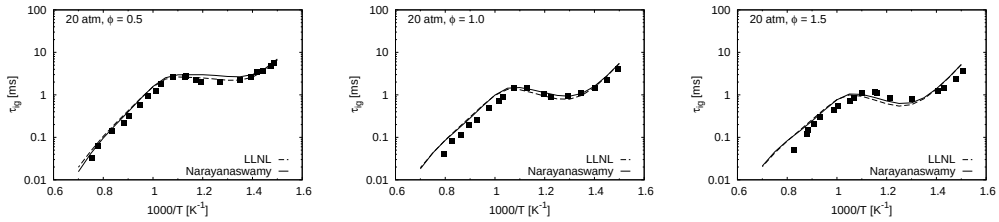

(a) $\phi = 0.5$ (b) $\phi = 1.0$ (c) $\phi = 1.5$

Figure 11: Ignition delay times of n-octane/air mixtures. Symbols denote experimental measurements [8]. Solid lines show numerical results for the base model from Narayanaswamy et al. [43], and dashed lines show the results for the base model from Sarathy et al. [8].

5. Mechanism development using optimized rate rules

This section explores how the optimized rate rules perform in the chemical mechanisms for larger alkanes that were not a part of the training set. n-Dodecane is chosen as the test case here, since data from various experimental configurations are available for this fuel, which enables an extensive validation of the developed model. In the following, an n-dodecane mechanism was derived using the rate rules calibrated in the previous section. This mechanism is compared with experimental measurements, a well-validated mechanism from the published literature [43], and a mechanism developed with the rate rules suggested in Refs. [8, 27, 56]. This allows for the assessment of the reliability and predictive quality of the optimized rate rules.

Two kinetic mechanisms were developed here for the combustion of n-dodecane. Consistent with the model development process in Section 3, the n-dodecane part in the LLNL mechanism [8] served as the starting point and was updated according to Bugler et al. [27] and Sivaramakrishnan and Michael [56]. This proposed mechanism includes the up-to-date kinetic knowledge and the rate rules [8, 27, 56] prior to the optimization. By replacing the unoptimized rate rules with those optimized in Section 4, the second n-dodecane mechanism was generated. Figure 12 shows the numerical results for these two mechanisms. The application of the optimized rate rules results in a significant improvement of model performance for the entire range of temperatures. The prediction uncertainties of the mechanism with the optimized rate rules are shown in the Supplementary material. The uncertainties were calculated based on the Monte Carlo method with the samplings generated during the UQ process. Detailed information for this calculation can be found in the Supplementary material.

In Fig. 13, the n-dodecane mechanism using the optimized rate rules is compared with a well-validated mechanism recently published by Narayanaswamy et al. [43]. The mechanism [43] was developed based on an extensive validation against measurements for various experimental configurations. However, the new mechanism based on the optimized rate rules shows more accurate predictions compared to the experimental data. More importantly, the modified mechanism reflects correctly the influence of equivalence ratio on the ignition delays in the low temperature range. The strongly reduced ignition delay times at low temperatures for n-dodecane are a major improvement and where also expected as reported by Pei et al. [70], who stated that the models

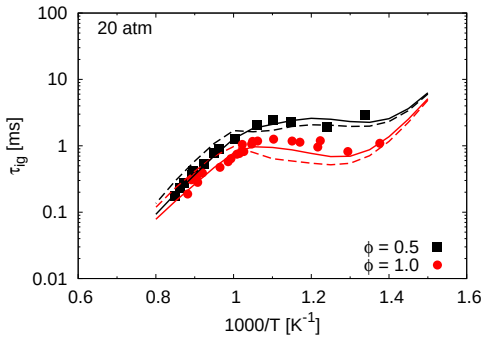

Figure 12: Ignition delay times of n-dodecane/air mixtures. Symbols denote experimental measurements [71]. Solid lines show the results for the model developed with the optimized rate rules, and dashed lines show the results for the model with the unoptimized rate rules [8, 27].

available in the literature ignite comparatively slowly in CFD simulations for spray experiments.

Additional comparison cases between the two models are presented in Figs. 14–19. Figures 14 and 15 show the concentrations of stable species measured in pressurized flow reactor configurations for stoichiometric n-dodecane/O_2/N_2 mixtures [72] and for lean n-dodecane/air mixtures [73], respectively. The discrepancies between experiment and simulation shown in Fig. 15 are mainly linked to the base chemistry, as analyzed in Ref. [43]. Malewicki and Brezinsky [74] measured the mole fractions of species for the oxidation of n-dodecane in a high pressure shock tube. The profiles of the reactants n-dodecane and O_2 are presented in Fig. 16, along with the data for some intermediate species, e. g. methane and acetylene. Figures 17 and 18 show the measurements for the pyrolysis of n-dodecane [74] and the oxidation of diluted n-dodecane/O_2/argon mixtures [75]. Discrepancies between

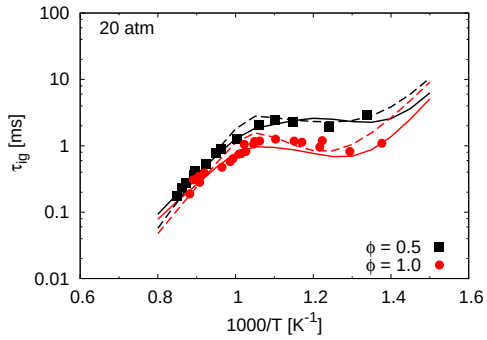

Figure 13: Ignition delay times of n-dodecane/air mixtures. Symbols denote experimental measurements [71]. Solid lines show the results for the model developed with the optimized rate rules, and dashed lines show the results for the model from Narayanaswamy et al. [43].

the model and the highly diluted oxidation measurements obtained at low pressures and high temperatures can be attributed to the fact that data under similar conditions for other n-alkanes were not utilized in the optimization process for rate rules. Data obtained under these conditions are primarily sensitive to unimolecular fuel decomposition reactions [76], which were not significantly optimized in the present work. The stable species concentration profiles during the oxidation of n-dodecane were measured in a jet stirred reactor by Ahmed et al. [69]. These data are shown in Fig. 19 in comparison with the simulation results. While the rate rules are optimized against shock tube measurements, data from various experimental configurations are taken into account here. For the most cases, the model with the optimized rate rules shows better agreement with experimental data.

The newly developed n-dodecane mechanism with the optimized rate rules gives satisfactory results. This is because the rate rules optimized based on experimental data of C_7–C_{11} normal alkanes inherently capture the

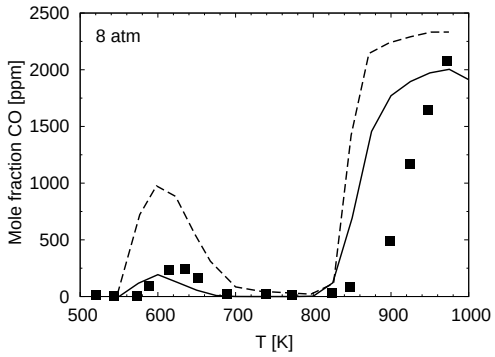

Figure 14: CO profiles of n-dodecane/O_2/N_2 (250/4625/995125 ppm) mixture combustion in a pressurized flow reactor at 8 atm with a residence time of 1 s. Symbols denote experimental measurements [72]. Solid lines show the results for the model developed with the optimized rate rules, and dashed lines show the results for the model from Narayanaswamy et al. [43].

analogous chemical kinetic features of n-dodecane. Therefore, the similarity in global oxidation behavior n-alkanes can be utilized to extract knowledge from shorter n-alkanes to benefit the development of kinetic models for longer n-alkanes such as n-dodecane. It is clearly demonstrated here that optimized rate rules improve the model performance when applied to derive models for larger hydrocarbons.

6. Concluding remarks

In this study, optimized rate rules for model development of normal alkanes are proposed. A chemical mechanism for C_7–C_{11} n-alkanes was first developed by updating a published mechanism [8] according to the suggestions of Bugler et al. [27]. The resulting mechanism uses consistent rate rules for all of these fuels. It was then subjected to an automatic model

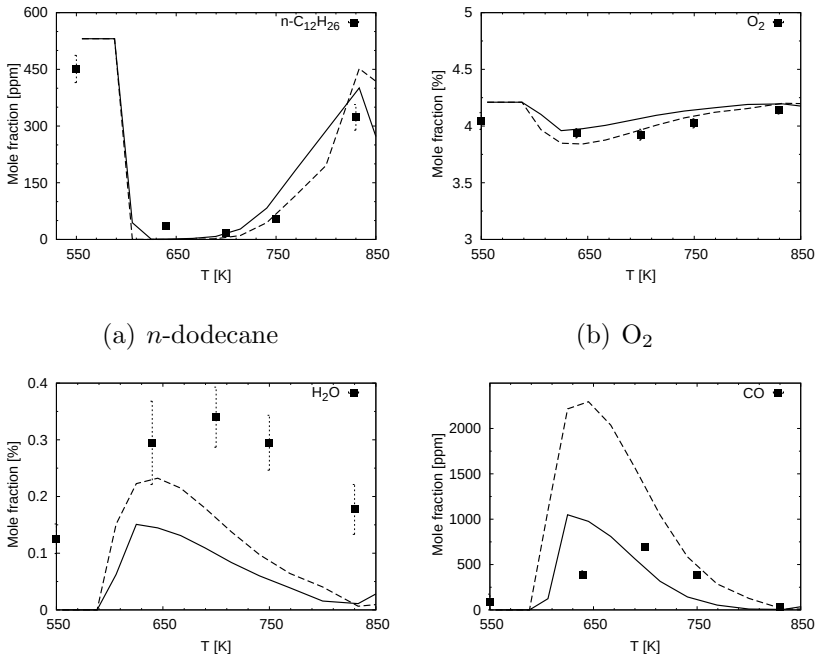

(a) *n*-dodecane (b) O_2

(c) H_2O (d) CO

Figure 15: Stable species profiles of lean ($\phi = 0.23$) oxidation of *n*-dodecane/air mixtures in a pressurized flow reactor at 8 atm with a residence time of 0.12 s. Symbols denote experimental measurements [73]. Solid lines show the results for the model developed with the optimized rate rules, and dashed lines show the results for the model from Narayanaswamy et al. [43].

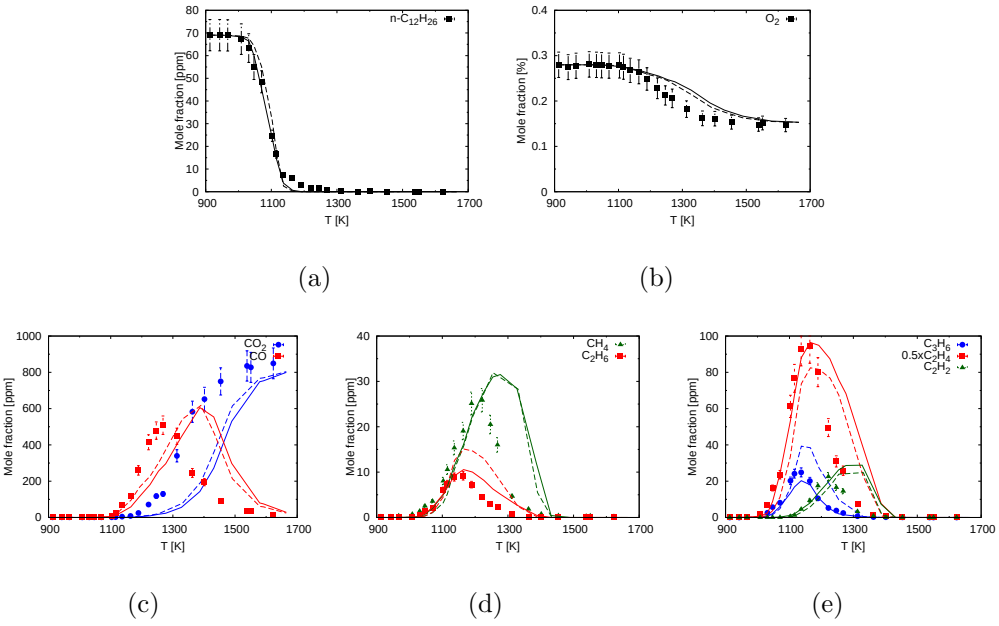

Figure 16: Stable species profiles of lean ($\phi = 0.46$) oxidation of n-dodecane/air mixtures in a shock tube at a pressure of 50 atm. Symbols denote experimental measurements [74]. Solid lines show the results for the model developed with the optimized rate rules, and dashed lines show the results for the model from Narayanaswamy et al. [43].

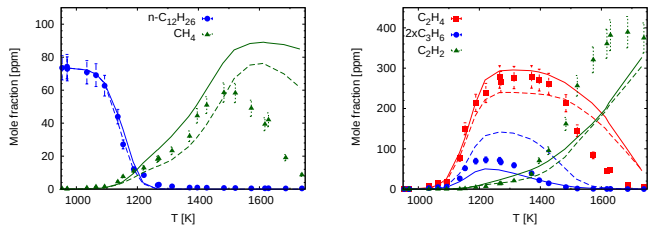

Figure 17: Stable species profiles of n-dodecane pyrolysis in a shock tube at a pressure of 22 atm [74]. Solid lines show the results for the model developed with the optimized rate rules, and dashed lines show the results for the model from Narayanaswamy et al. [43].

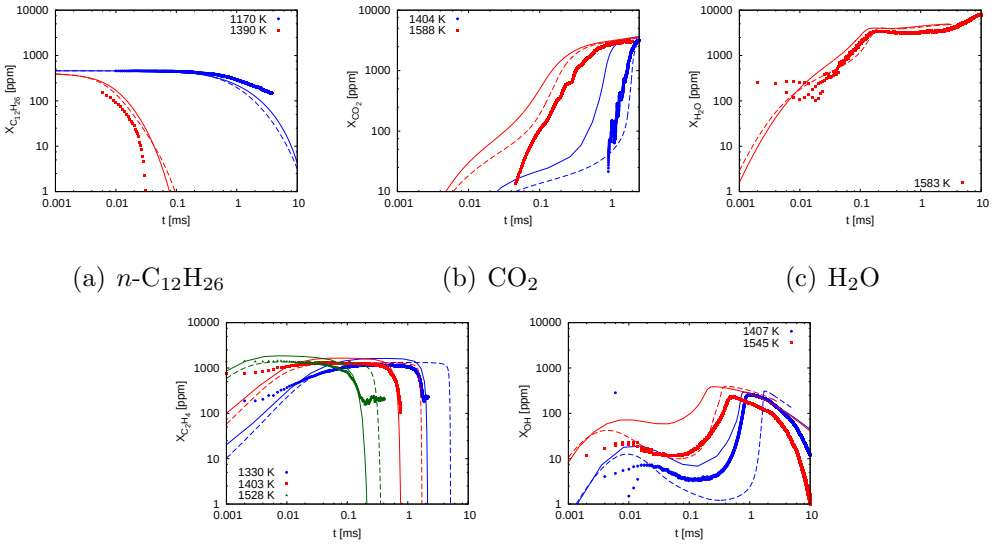

(a) n-$C_{12}H_{26}$ (b) CO_2 (c) H_2O

(d) C_2H_4 (e) OH

Figure 18: Species mole fractions of stoichiometric oxidation of n-dodecane/O_2/Ar mixtures in a shock tube at 2.25 atm. Symbols denote experimental measurements [75]. Solid lines show the results for the model developed with the optimized rate rules, and dashed lines show the results for the model from Narayanaswamy et al. [43].

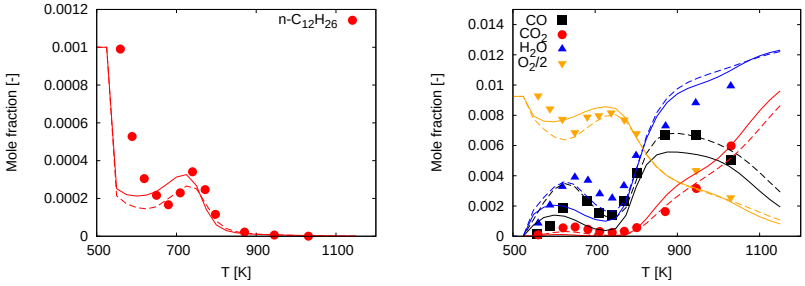

(a) (b)

Figure 19: n-dodecane oxidation in a JSR at 10 bar, $\tau = 1.0$ s, and $\phi = 1.0$. The initial fuel mole fraction is 1000 ppm. Symbols denote the experimental data [69]. Solid lines show the results for the model developed with the optimized rate rules, and dashed lines show the results for the model from Narayanaswamy et al. [43].

optimization against a large number of experimental measurements, where a Bayesian framework was applied to extract information from experiments for different fuels to update the knowledge about rate rules. Excellent agreement between simulations and experiments was achieved for the oxidation of C_7–C_{11} *n*-alkanes using the updated rate rules again consistently for all fuels. After this successful training, the optimized rate rules were applied to derive a chemical mechanism for *n*-dodecane, which was not used as part of the training set. The proposed mechanism matches experimental data from various experimental configurations over a variety of conditions well. Compared with a mechanism using the unoptimized rate rules and a well-validated mechanism from the published literature [43], the mechanism developed with the calibrated rate rules shows substantially improved prediction accuracy. Overall, it is demonstrated in the present study that the rate rules optimized for a set of smaller hydrocarbon fuels are able to give satisfactory model performance when applied in the model development for larger hydrocarbon fuels.

This work presents a new approach for the development of chemical kinetic models, where models are first developed/updated using state-of-the-art thermochemistry and reaction rate rules that draw from experiments and theory-based computations. The combination of fundamental knowledge of chemical kinetic modeling with information gained with the aid of uncertainty quantification methods enables the development of more accurate chemical kinetic models.

Acknowledgments

This work was performed within the Cluster of Excellence "Tailor-Made Fuels from Biomass", which is funded by the Excellence Initiative of the German federal state governments to promote science and research at German universities. The authors also acknowledge funding support from the Clean Combustion Research Center and Saudi Aramco under the FUELCOM program. We would like to thank Dr. Krithika Narayanaswamy, Mr. Leif Kröger, and Mr. Christoph Thies for their support with numerical calculations and Dr. Sungwoo Park (KAUST) for his help with developing the kinetic model.

References

[1] S. Honnet, K. Seshadri, U. Niemann, N. Peters, Proc. Combust. Inst. 32 (2009) 485-492

[2] T. Malewicki, S. Gudiyella, K. Brezinsky, Combust. Flame 160 (2013) 17-30

[3] H. Shen, J. Steinberg, J. Vanderover, M. Oehlschlaeger, Energ Fuel 23 (2009) 2482-2489

[4] S.M. Sarathy, T. Javed, F. Karsenty, A. Heufer, W. Wang, S. Park, A. Elwardany, A. Farooq, C.K. Westbrook, W.J. Pitz, M.A. Oehlschlaeger, G. Dayma, H.J. Curran, P.Dagaut, Combust. Flame 161 (2014) 1444-1459

[5] H. Curran, P. Gaffuri, W. Pitz, C. Westbrook, Combust. Flame 114 (1998) 149-177

[6] H. Curran, P. Gaffuri, W. Pitz, C. Westbrook, Combust. Flame 129 (2002) 253-280

[7] C.K. Westbrook, W.J. Pitz, O. Herbinet, H.J. Curran, E.J. Silke, Combust. Flame 156 (2009) 181-199

[8] S.M. Sarathy, C.K. Westbrook, M. Mehl, W. J. Pitz, C. Togbé, P. Dagaut, H. Wang, M.A. Oehlschlaeger, U. Niemann, K. Seshadri, P.S. Veloo, C. Ji, F.N. Egolfopoulos, T. Lu, Combust. Flame 158 (2011) 2338-2357

[9] S.M. Sarathy, S. Vranckx, K. Yasunaga, M. Mehl, P. Owald, W.K. Metcalfe, C.K. Westbrook, W.J. Pitz, K. Kohse-Höinghaus, R.X. Fernandes, H.J. Curran, Combust. Flame 159 (2012) 2028-2055

[10] L. Cai, A. Sudholt, D.J. Lee, F.N. Egolfopoulos, H. Pitsch, C.K. Westbrook, S.M. Sarathy, Combust. Flame 161 (2014) 798-809

[11] L. Cai, Y. Uygun, C. Togbé, H. Pitsch, H. Olivier, P. Dagaut, S.M. Sarathy, Proc. Combust. Inst. 35 (2015) 419-427

[12] W.H. Green, J.W. Allen, R.W. Ashcraft, G.J. Beran, C.A. Class, C. Gao, C.F. Goldsmith, M.R. Harper, A. Jalan, G.R. Magoon, D.M. Matheu, S.S. Merchant, J.D. Mo, S. Petway, S. Raman, S. Sharma, J. Song, K.M. Van Geem, J. Wen, R.H. West, A. Wong, H. Wong, P.E. Yelvington, J. Yu, RMG Reaction Mechanism Generator Version 3.3, http://rmg.sourceforge.net/.

[13] P.A. Glaude, F. Battin-Leclerc, R. Fournet, V. Warth, G.M. Cóme, G. Scacchi, Combust. Flame 122 (2000) 451-462

[14] C. Zhou, J.M. Simmie, H.J. Curran, Combust. Flame 158 (2011) 726-731

[15] C. Zhou, J.M. Simmie, H.J. Curran, Phys. Chem. Chem. Phys. 12 (2010) 7221-7233

[16] S. Di Tommaso, P. Rotureau, O. Crescenzi, C. Adamo, Phys. Chem. Chem. Phys. 13 (2011) 14636-14645

[17] Z. Zhao, M. Chaos, A. Kazakov, F.L. Dryer. Int. J. Chem. Kin. 40 (1) (2008) 1-18

[18] A.V. Joshi, H. Wang. Int. J. Chem. Kin. 38 (2006) 57-73

[19] V. Vasudevan, D.F. Davidson, R.K. Hanson, J. Phys. Chem. A. 109 (2005) 3352-3359

[20] S.S. Vasu, Z. Hong, D.F. Davidson, R.K. Hanson, D.M. Golden, J. Phys. Chem. A. 114 (2010) 11529-11537

[21] R. Sivaramakrishnan, J.V. Michael, Combust. Flame 156 (2009) 1126-1134

[22] A. Miyoshi, Int. J. Chem. Kin. 44 (2012) 59-74

[23] S.M. Villano, L.K. Huynh, H.-H. Carstensen, A.M. Dean, J. Phys. Chem. A 115 (2011) 13425-13442

[24] S.M. Villano, L.K. Huynh, H.-H. Carstensen, A.M. Dean, J. Phys. Chem. A 116 (2012) 5068-5089

[25] A. Miyoshi, J. Phys. Chem. A 115 (2011) 3301-3325

[26] S. Sharma, S. Raman, W.H. Green, J. Phys. Chem. A 114 (2010) 5689-5701

[27] J. Bugler, K.P. Somers, E.J. Silke, H.J. Curran, J. Phys. Chem. A 119 (2015) 7510-7527

[28] C.F. Goldsmith, W.H. Green, S.J. Klippenstein, J. Phys. Chem. A 116 (2012) 3325-3346

[29] L.K. Huynh, H.H. Carstensen, A.M. Dean, J. Phys. Chem. A 114 (2010) 6594-6607

[30] C.Y. Sheng, J.W. Bozzelli, A.M. Dean, A.Y. Chang, J. Phys. Chem. A 106 (2002) 7276-7293

[31] J.A. Miller, S.J. Klippenstein, S.H. Robertson, Proc. Combust. Inst. 28 (2000) 1479-1486

[32] J.A. Miller, S.J. Klippenstein, Int. J. Chem. Kin. 33 (2001) 654-668

[33] J.D. DeSain, S.J. Klippenstein, J.A. Miller, C.A. Taatjes, J. Phys. Chem. A 107 (2003) 4415-4427

[34] H. Sun, J.W. Bozzelli, J. Phys. Chem. A 108 (2004) 1694-1711

[35] M. Frenklach. Combust. Flame 58 (1984) 69-72

[36] M. Frenklach, A. Packard, P. Seiler, R. Feeley, Int. J. Chem. Kin. 36 (2004) 57-66

[37] D.A. Sheen, H. Wang. Combust. Flame 158 (2011) 2358-2374

[38] M.T. Reagan, H.N. Najm, R.G. Ghanem, O.M. Knio. Combust. Flame 132 (3) (2003) 545-555

[39] H. Wang, D.A. Sheen, Progress in Energy and Combustion Science 47 (2015) 1-31

[40] L. Cai, H. Pitsch, Combust. Flame 161 (2014) 405-415

[41] M. Frenklach, D.W. Clary, Twentieth Symposium (International) on Combustion (1984) 887-901

[42] L. Cai, H. Pitsch, Combust. Flame 162 (2015) 1623-1637

[43] K. Narayanaswamy, P. Pepiot, H. Pitsch, Combust. Flame 161 (2014) 866-884

[44] R.T. Cox, The Algebra of Probable Inference, Johns Hopkins University Press, Baltimore, MD, (1961)

[45] E.T. Jaynes, Probability Theory: The Logic of Science, Cambridge University Press, Cambridge, (2003)

[46] K. Braman, T.A. Oliver, V. Raman, Combustion Theory and Modelling 17 (2013) 858-887

[47] J. Prager, H.N. Najm, K. Sargsyan, C. Safta, W.J. Pitz, Combust. Flame 160 (2013) 1583-1593

[48] E. Prudencio, K.W. Schulz, Workshop on Algorithms and Programming Tools for Next-Generation High-Performance Scientific Software (HPSS), Bordeaux, France, 2011

[49] S. Mosbach, J.H. Hong, G.P.E. Brownbridge, M. Kraft, S. Gudiyella, K. Brezinsky, Int. J. Chem. Kin. 46 (2014) 389-404

[50] K. Miki, E.E. Prudencio, S.H. Cheung, G. Terejanu, Combust. Flame. 160 (2013) 861-869

[51] S. G. Davis, A. B. Mhadeshwar, D. G. Vlachos, H. Wang, Int. J. Chem. Kinet. 36 (2004) 94-106

[52] H. Pitsch, FlameMaster: A C++ computer program for 0D combustion and 1D laminar flame calculations

[53] S.M. Burke, J.M. Simmie, H.J. Curran, J. Phys. Chem. Ref. Data 44 (2015) 013101

[54] S.W. Benson, Thermochemical Kinetics, 2nd ed.; Wiley: New York (1976)

[55] E.R. Ritter, J.W. Bozzelli, THERM: Thermodynamic Property Estimation for Gas Phase Radicals and Molecules. Int. J. Chem. Kin. 23 (1991) 767-778

[56] R. Sivaramakrishnan, J.V. Michael, J. Phys. Chem. A 113 (2009) 5047-5060

[57] P. Pepiot-Desjardins, H. Pitsch, Combust. Flame, 154 (2008) 67-81

[58] U. Pfahl, K. Fieweger, G. Adomeit, Proc. Combust. Inst. 26 (1996) 781-789

[59] M.F. Campbell, S. Wang, C.S. Goldenstein, R.M. Spearrin, A.M. Tulgestke, L.T. Zaczek, D.F. Davidson, R.K. Hanson, Proc. Combust. Inst. 35 (2015) 231-239

[60] H.K. Ciezki, G. Adomeit Combust. Flame 93 (1993) 421-433

[61] V.P. Zhukov, V.A. Sechenov, A.Yu. Starikovski, Combust. Flame 153 (2008) 130-136

[62] B. Rotavera, E.L. Petersen, Shock Waves 23 (2013) 345-359

[63] D.F. Davidson, S.C. Ranganath, K.-Y. Lam, M. Liaw, Z. Hong, R.K. Hanson, J. Prop. Power (26) 2010

[64] A. Chakir, M. Bellimam, J.C. Boettner, Cathonnet, Int. J. Chem. Kin. 24 (1992) 385-410

[65] O. Herbinet, B. Husson, Z. Serinyel, M. Cord, V. Warth, R. Fournet, P. Glaude, B. Sirjean, F. Battin-Leclerc, Z. Wang, M. Xie, Z. Cheng, F. Qi, Combust. Flame 159 (2012) 3455-3471

[66] F.L. Dryer, K. Brezinsky, Combustion Science and Technology 45 (1986) 199-212

[67] S.P. Zeppieri, S.D. Klotz, F.L. Dryer, Proc. Combust. Inst. 28 (2000) 1587-1595

[68] G. Mittal, M.P. Raju, C.-J. Sung, Combust. Flame 157 (2010) 1316-1324

[69] A, Mzé-Ahmed, K. Hadj-Ali, P. Dagaut, G. Dayma, Energy Fuels 26 (2012) 4253-4268

[70] Y. Pei, E.R. Hawkes, S. Kook, G.M. Goldin, T. Lu, Combust. Flame 162 (2015) 2006-2019

[71] S.S. Vasu, D.F. Davidson, Z. Hong, V. Vasudevan, R.K. Hanson, Proc. Combust. Inst. 32 (2009) 173-180

[72] P.S. Veloo, S. Jahangirian, F.L. Dryer, Spring Technical Meeting, Central States Section of the Combustion Institute (2012)

[73] M.S. Kurman, R.H. Natelson, N.P. Cernansky, D.L. Miller, Proc. Combust. Inst. 33 (2011) 159-166

[74] T. Malewicki, K. Brezinsky, Proc. Combust. Inst., 34 (2013) 361-368

[75] D.F. Davidson, Z. Hong, G.L. Pilla, A. Farooq, R.D. Cook, R.K. Hanson, Proc. Combust. Inst. 33 (2011) 151-157

[76] S.S. Vasu, S.M. Sarathy, Energy Fuels 27 (2013) 7072-7080

Supplementary Material

Click here to download Supplementary Material: Package_400.zip

Supplementary Material

Click here to download Supplementary Material: Readme

Supplementary Material

Click here to download Supplementary Material: supplementary.pdf

Thermo data in FlameMaster format

Click here to download Supplementary Material: nalkanes.thermo

Transport data in FlameMaster format

Click here to download Supplementary Material: nalkanes.trans

Mechanism in FlameMaster format

Click here to download Supplementary Material: nalkanes.mech

Thermo data in Chemkin format

Click here to download Supplementary Material: nalkanes.chthermo

Mechanism in Chemkin format

Click here to download Supplementary Material: nalkanes.chmech

Transport data in Chemkin format

Click here to download Supplementary Material: nalkanes.chtrans